Appendix G

The following technical supplement was prepared by Drew Canfield to provide a detailed explanation of the scientific analysis in Chapter 2 of this report.

Technical Supplement for the Analysis of the Battle of Rhode Island in August 1778

Drew Canfield, Roger Williams University

Summary of the Battle at Valley Road

The British held Newport in 1778 during the Revolutionary War, which was a seaport capable of providing the British with units and needed supplies. In the same year, a treaty with France aligned the French with the Colonials in the war. Admiral d'Estaing commanded a fleet of twelve ships to aid the Colonials in the war. At the request of General Washington, Admiral d'Estaing was reassigned to aid General Sullivan in the removal of the British in Newport. General Pigot, in charge of the British Forces, sought to defend Newport due to its value as a seaport. Armed with reports of the French's aid and marching orders for General Sullivan on Newport, General Pigot called his units to pull back and fortify Newport. Defensive fortifications, including the structures redoubt and abbatis, were constructed by the British to hold the seaport. The abbatis ran from Green End to Tonomy Hill, defense working 4 feet high and 6 feet deep, about 40 feet behind the abbatis. The Colonial troops stationed themselves in Portsmouth, and intended on marching to Honeyman Hill to combat Card's Redoubt on Valley Road. A map of the battlefield can be seen in Figure 4.

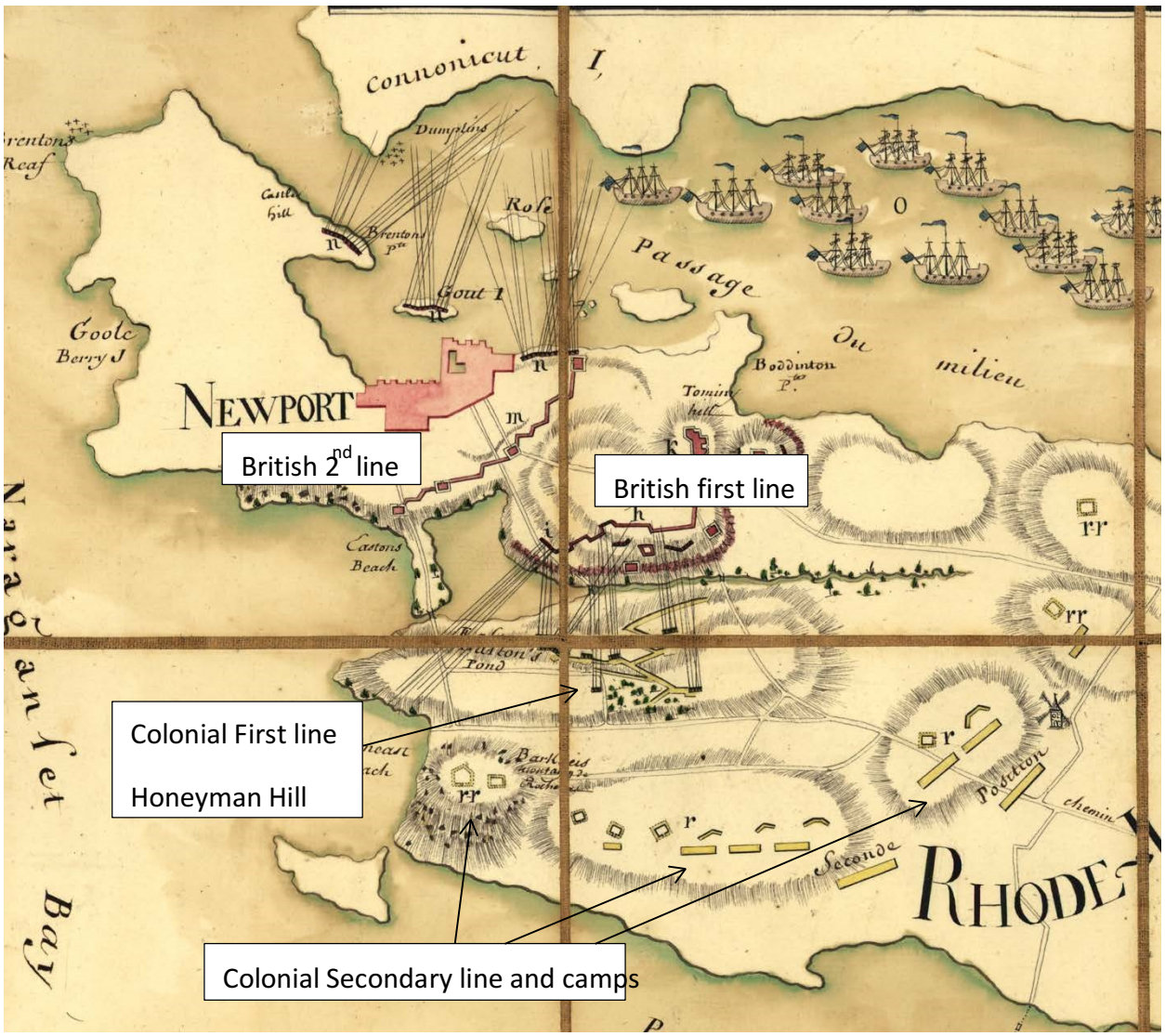

Figure 4: Map of battlefield at Valley Road. Positions of Combatants noted.

The colonials held smooth bore cannons, which featured a maximum range of 2000 yards, yet were most effective at ranges less than 1000 yards. While their elevated position at Honeyman Hill provided an advantage due to elevation (176 feet), the distance between the emplacements and the British' Card's Redoubt was 1700 yards, elevated 74 feet high. There was also a 10 Gun battery at a range of 1800 yards and a height of 113 feet. Gail winds and rain caused Eastons Pond, which bordered the British encampments, to increase and size, and turned surrounding terrain into a marsh; therefore, Colonial maneuverability was decreased.

Records by Captain Mackenzie of the British in his diary reveal that cannon fire did not result in irreparable damage to British artillery and defenses. General Washington ordered the Colonials to retreat on August 28, 1778 due to the lack of progress. While the failure of the battle can be partially attributed to the lack of an element of surprise due to the lack of cover for arriving French Naval ships, and the delivery of a letter from Colonial Generals telling General Pigot of their incoming attack, a question remains: why were the cannons fired by the Colonials incapable of destroying British artillery and defenses? This technical report aimed to analyze the ballistics of cannon fire during the era of the Revolutionary War through simulation in order to uncover potential explanations for the loss.

For a more thorough analysis of the battle, including tactics, details of the terrain, and other details including references, please refer to the historical evaluation which this supplement accompanies.

Cannon fire Simulation Theory

Internal Ballistics Theory

Cannon fire and associated ballistics is a relatively understudied field when compared to other weapon ballistics studies, such as rifles, missiles, etc. Benjamin Robins, a military engineer and mathematician, developed an analytical model for internal ballistics for cannon fire in 1742 (Robins 1805). Robins claimed that the force exerted on the cannonball traveling down the muzzle can be approximated using the following equation:

$$F(x) = \frac{RP_{atm}Ac}{x}$$

Equation 1: Force exerted on cannonball due to expansion of gas from gunpowder ignition in a cannon muzzle from Robins 1805.

where:

F(x): force exerted on the cannonball

R: initial ratio of hot gas pressure to atmospheric pressure

P_{atm}: atmospheric pressure

A: cross-sectional area of the cannon-ball

C: length of the barrel occupied by the powder charge prior to ignition

The Australian Research Council (ARC), specifically Dr. Collins, reviewed Robin's work, as well as work done by others, to derive models for analyzing smooth bore cannon ballistics (Collins n.d.). Robin's research also discussed the air resistance experienced by the cannonball as it accelerates, as well as models for approximating the velocity of the cannonball. As the ARC states, Newton's second law (Equation 2) can be utilized to derive an expression for the velocity of the ball (Equation 3).

$$F = ma$$

Equation 2: Newton's Second Law

where:

F: Force

m: mass of the body

a: acceleration of the body

$$\frac{1}{2}mv^2 = \int_c^L F(x)dx$$

Equation 3: Kinetic energy of the cannonball in terms of the work done on the ball derived from Newton's Second Law

where:

m: mass of the cannonball

v: muzzle velocity of the cannonball at a distance L down the barrel

L: full length of the barrel

The left-hand term is the kinetic energy of the cannonball, while the right-hand integral is the work done on the ball. Substituting Equation 1 into Equation 3 and solving the integral results in Equation 4.

$$\frac{1}{2}mv^2 = RP_{atm}Acln\left(\frac{L}{c}\right)$$

Equation 4: Solution to the integral shown in Equation 3.

The cross-sectional area of a cannonball can be modeled as a circle, and the length of barrel occupied by powder charge can be approximated using the density of gunpowder, as shown by ARC in Equation 5.

$$P = \frac{\pi d^2 c}{4}\eta$$

Equation 5: Mass of the powder charge in terms of density

where:

P: Powder Charge

η: Gunpowder density

d: diameter of cannonball

Rearranging Equation 5 and substituting into Equation 4 yields Equation 6.

$$\frac{1}{2}mv^2 = RP_{atm}\left(\frac{\pi d^2}{4}\right)\left(\frac{4P}{\eta\pi d^2}\right)ln\left(\frac{L}{c}\right)$$

Equation 6: Full expression for kinetic energy as a function of work done on a cannonball in the muzzle of a cannon

Again, rearranging and simplifying Equation 6 in terms of muzzle velocity results in an expression capable of approximating muzzle velocity (Equation 7).

$$v = \sqrt{\frac{2RP_{atm}}{m}\left(\frac{P}{\eta}\right) ln\left(\frac{L}{c}\right)}$$

Equation 7: Muzzle velocity of a cannonball exiting a cannon

External Ballistics Theory

Dr. Collins also outlines the ballistics acting upon a cannonball external to the cannon. The main force acting to decelerate the cannonball is aerodynamic drag acting on the surface of the cannonball (Equation 8).

$$F_D = \frac{1}{2} C_D \rho A v^2$$

Equation 8: Drag force acting on an objecting traveling through a fluid

where:

F_D: Force of drag acting on the cannonball

C_D: Coefficient of drag

ρ: Density of the fluid through which the body is traveling

v: velocity of the body

Note that this analytical model neglects viscous drag, which is an appropriate assumption for objects with high Reynolds numbers. Reynolds number is a non-dimensional parameter for

comparing the inertial forces, or similarly pressure drag, of the object moving through the fluid to the viscous forces impeding it (Equation 9). The higher the Reynolds number, the less viscous drag forces impact the object. Fluids with a Reynolds number below 2300 are considered laminar, transitional between 2300 and 4000, and turbulent above 4000.

$$Re = \frac{\rho v L}{\mu}$$

Equation 9: Reynolds number

where:

Re: Reynolds Number

L: Hydraulic diameter of the object

μ: Kinematic viscosity of the fluid

Note that the hydraulic diameter of a circle is the diameter of that circle. The Reynolds number of the cannonballs in flight will be calculated in the simulation to verify this assumption. The drag coefficient of an object is dependent on the geometry of the object, the surface roughness, fluid properties, and the velocity of the fluid passing over the object. A model developed by Spearman and Braswell for the drag coefficient of a sphere for Mach numbers, or ratio of current velocity to the speed of sound (1125.33 feet/second), between 0.6 and 10.5 was utilized for approximating the drag coefficient on the cannonball (Spearman and Braswell 1993).

J. W. M. Bush in the department of mathematics at MIT impresses the importance of considering another phenomenon termed the drag crisis when modeling drag forces acting on an object in flight (Bush 2013). While the viscous effects are negligible and the pressure drag is the most influential force on the ball in flight when looking at the system as a whole, within the layer of fluid adjacent to the ball, titled the boundary layer, the viscous forces play a larger role. Below

is a figure taken from Bush's report showing the progression of the boundary layer as the Reynolds number increases.

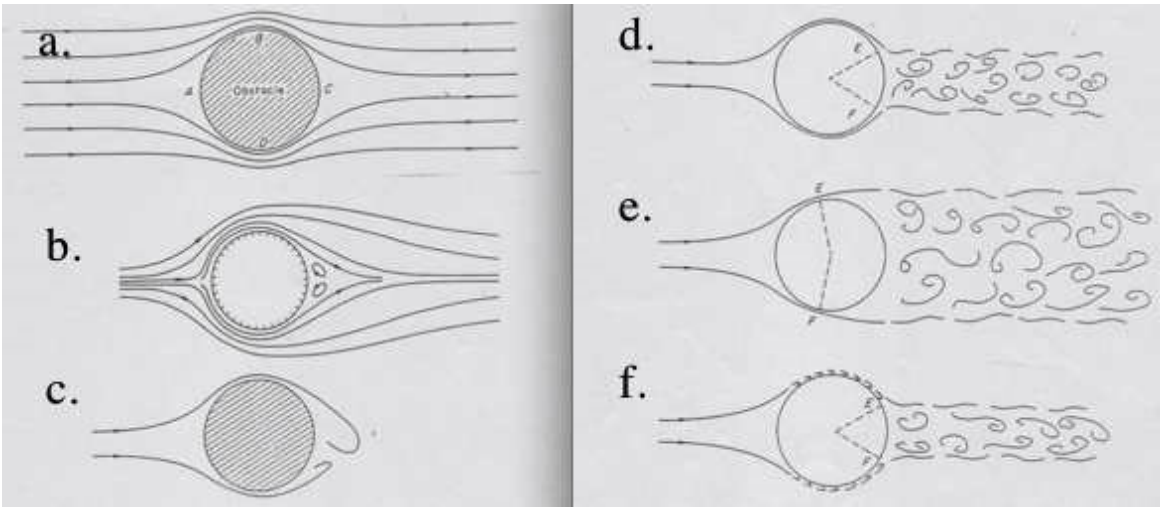

Figure 5: Figure 3 from Bush 2013. Caption reads as follows. Figure 3: Schematic illustration of the evolution of the flow past a smooth sphere with increasing Reynolds number, Re = Ua/v. a) For Re # 1, the streamlines are fore-aft symmetric and the drag is principally of viscous origins. b) For Re > 10, boundary layer separation downstream of the sphere induces a vortical wake and a significant pressure drag.c) For 100 < Re < 1000, the vortical wake becomes unstable, resulting in lateral forces on the sphere. d) For Re > 1000, the wake becomes turbulent, its extent being maximum for e) Re ≈ 2×10^5. f) For Re > 2×10^5, the boundary layers become turbulent, delaying the boundary layer separation and decreasing the extent of the turbulent wake. Owing to the resulting dramatic reduction in drag on the sphere, the latter transition is called the drag crisis. Note that the precise Re-values at which flow transitions occurs depends strongly on the sphere's surface roughness. Images from Daish (1972).

As shown in the transition from picture d to e to f in Figure 5, the boundary layer separates from the object with increasing Reynolds numbers and then conforms back to the surface geometry as Reynolds number continues to increase. A body experiencing fluid flow

with a Reynolds number between $2x10^5$ and $2x10^6$ experiences what is known as the drag crisis. In this range, the drag coefficient increases significantly before lowering again at higher Reynolds numbers. Again, the Reynolds number for the cannonball in flight needs to be calculated over the course of its flight to assess whether or not the cannonball experiences the drag crisis.

Zhang Lumin in the Foreign Technology Division report titled "Research on the Asymmetrical Aerodynamic Forces of Reentry Vehicles" states that asymmetric surface drag can impart a rotational acceleration upon a reentry vehicle (Lumin 1992). Asymmetric surface drag can be generated from asymmetric surface roughness. Rotational velocities of a body in flight within a fluid medium experience the Magnus effect, which can alter the trajectory of the ball depending on the axis about which the ball is rotating. J. W. M. Bush also enumerates the different effects the Magnus Effect can have on a ball's trajectory (Bush 2013). In summary, the cannonball could experience an acceleration in any direction, causing the ball to potential spread horizontally, or fall short of the target, or pass over the target.

David Poche and Peter George detail in their paper titled "Solid Shot Essentials: A guide to the Authentic and Non-Authentic" the formation of a mold seam and mold vent sprue from a solid shot mold on a cannonball, which would create asymmetric surface roughness ()Poche and George n.d.). Dr. Steve Jordan from the University of Rhode Island asserted that super-sonic bodies experience negligible accelerations resulting from surface roughness phenomena. Evaluation of the simulation would reveal the nature of the cannonball in flight and the necessity of including rotational acceleration into the simulation will be determined at that point. The Mach number can be used to determine this necessity.

MATLAB Code Rationale

Cannons with varying bores and associated gunpowder quantity and cannonball size were used in the simulation to observe the trajectory of the different cannons used in the 18th century. The first section of the code uses the equations for internal ballistics to approximate the velocity of the cannon at any point along the muzzle. The velocity and force acting on the cannonball are checked at one thousand positions within the muzzle.

The drag equations discussed in the external ballistics section were used to calculate the velocity at each point using Newton's second law. The equation itself can be rewritten in a differential form in terms of velocity, for acceleration is the first derivative of velocity (Equation 10). Position can also be derived from this expression, for velocity is the first derivative of position.

$$\frac{F}{m} = a = \frac{dv}{dt} = \frac{d}{dt}\left(\frac{dv}{dt}\right)$$

Equation 10: Differential form of Newton's Second law

The aerodynamic drag forces impart a deceleration on the ball; therefore, the velocity of the ball at any time can be approximated as the velocity of the point prior subtracted by the deceleration approximated by Equation 10, multiplied by the amount of time the object experienced that acceleration (Equation 11).

$$v_x(t_n) = v_x(t_{n-1}) - \frac{F_x(t_n)}{m} * dt$$

Equation 11: Approximation of the velocity of the cannonball heading downfield

This equation can be modified to include any other decelerating effects needed for simulation, such as gravity in the y-direction (Equation 12).

$$v_y(t_n) = v_y(t_{n-1}) - \frac{F_y(t_n)}{m} * dt - g * dt$$

Equation 12: Approximation of the velocity of the cannonball heading in the vertical direction

Total velocity of the cannonball at any point can be calculated using vectors and the Pythagorean Theorem (Equation 13).

$$V_{total}(t_n) = \sqrt{v_y(t_n)^2 + v_x(t_n)^2}$$

Equation 13: Total velocity of the cannonball at any point in time.

Given that the cannon is fired at an upward angle, the muzzle velocity must be separated into the vertical and downfield components based on the angle, θ, it was fired at (Equation 14).

$$v_y(0) = V_{muzzle}\sin(\theta), \qquad v_x(0) = V_{muzzle}\cos(\theta)$$

Equation 14: Vertical and downfield components of the cannonball velocity at the first instant the cannonball leaves the muzzle

The position of the ball over time after it leaves the muzzle will be approximated using the average of the velocity one point in the simulation prior to the current point and the current velocity (Equation 15). The position of the ball is checked for twelve thousand and 1 positions, at 0.001 second intervals.

$$y(t_n) = y(t_{n-1}) + \left(\frac{v_y(t_n) + v_y(t_{n-1})}{2}\right) * dt$$

Equation 15: Position of the cannonball at any time. Written in terms of the y-direction

This equation can be rewritten for the x or z-direction. The code also calculates the kinetic energy of the cannonball, as well as the Reynolds number of the fluid around the cannonball and the angle of attack of the cannonball. Angle of attack is defined as the arctangent

of the velocity in the y and x direction (Equation 16). The returned angle is the vertical angle at which the cannonball is ascending or descending.

$$\beta = \text{atan}\left(\frac{v_y(t_n)}{v_x(t_n)}\right)$$

Equation 16: Angle of attack of the cannonball

Once the simulation has run, the time and position downfield at which the cannonball lands can be determined. Note that the altitude would be set as -200 feet for the cannon is fired at an elevated position and fired at a 4 degree angle. Internal and external ballistics are plotted over position, including velocities, forces, Reynolds numbers, Mach numbers and kinetic energy. All code can be seen in the Appendix.

Results for Cannon Fire Simulation

Validation of Assumptions

The minimum Mach number for muzzle velocities of the different cannons fired was 1.164, meaning the ball is exiting the muzzle at supersonic speed; therefore, neglecting asymmetric surface roughness is a valid assumption. The minimum Reynolds number of the cannonballs during flight was 9.42×10^5; therefore, the drag crisis occurs within the muzzle and does not occur during flight. Additionally, the airflow around the cannonball is turbulent, meaning the viscous drag is negligible compared to the pressure drag.

Internal Ballistics Plots

Below are two plots, one showing the force exerted on the cannonball over the length of the cannon (Figure 6) and the other showing the Mach number of the cannonball over the length of the cannon (Figure 7).

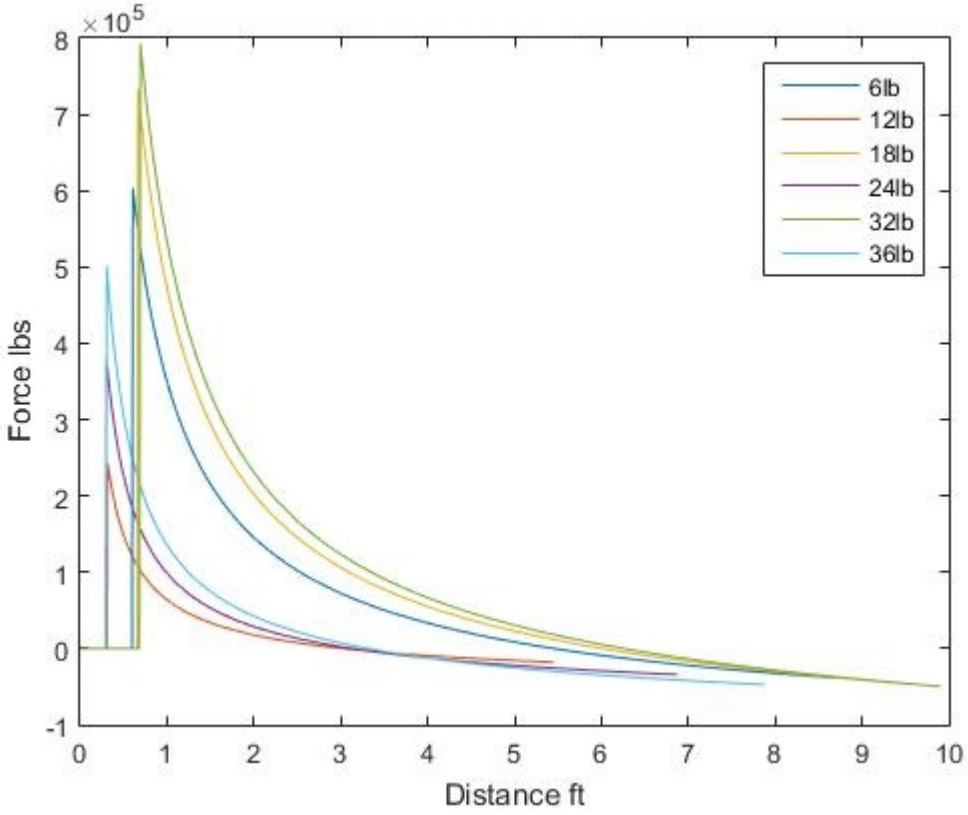

Figure 6: Force exerted on the cannonball over the length of the cannon. Legend shows weight of cannonballs

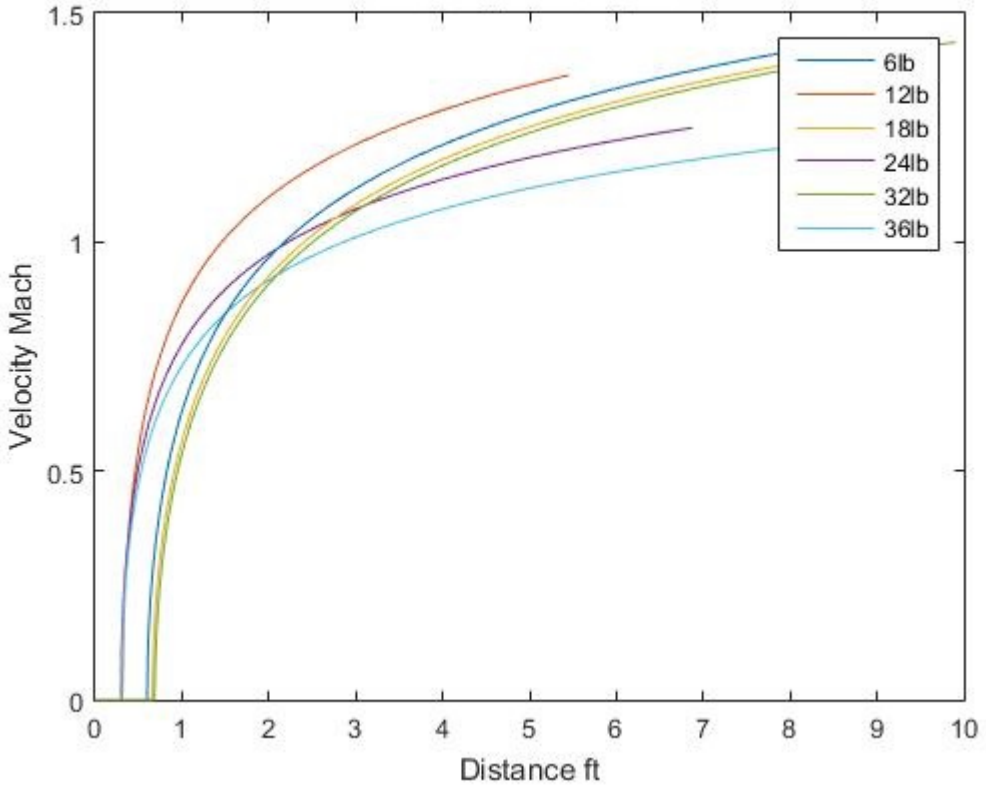

Figure 7: Mach number of the cannonball over the length of the cannon. Legend shows weight of cannonballs

External Ballistics Results

Below are the plots from the external ballistics simulation. Each of the following figures were plotted against the distance downfield the cannonball currently achieved at each point. Figure 8 shows the altitude of the cannonball. Figure 9 shows the angle of attack of the cannonball. Figure 10 shows the kinetic energy of the cannonball. Figure 11 shows the Reynolds number of the cannonball. Figure 12 shows the total velocity of the cannonball. Figure 13 shows the x-component velocity of the cannonball. Figure 14 shows the y-component of the cannonball. Finally, Figure 15 shows the coefficient of drag for a cannonball as a function of Mach number.

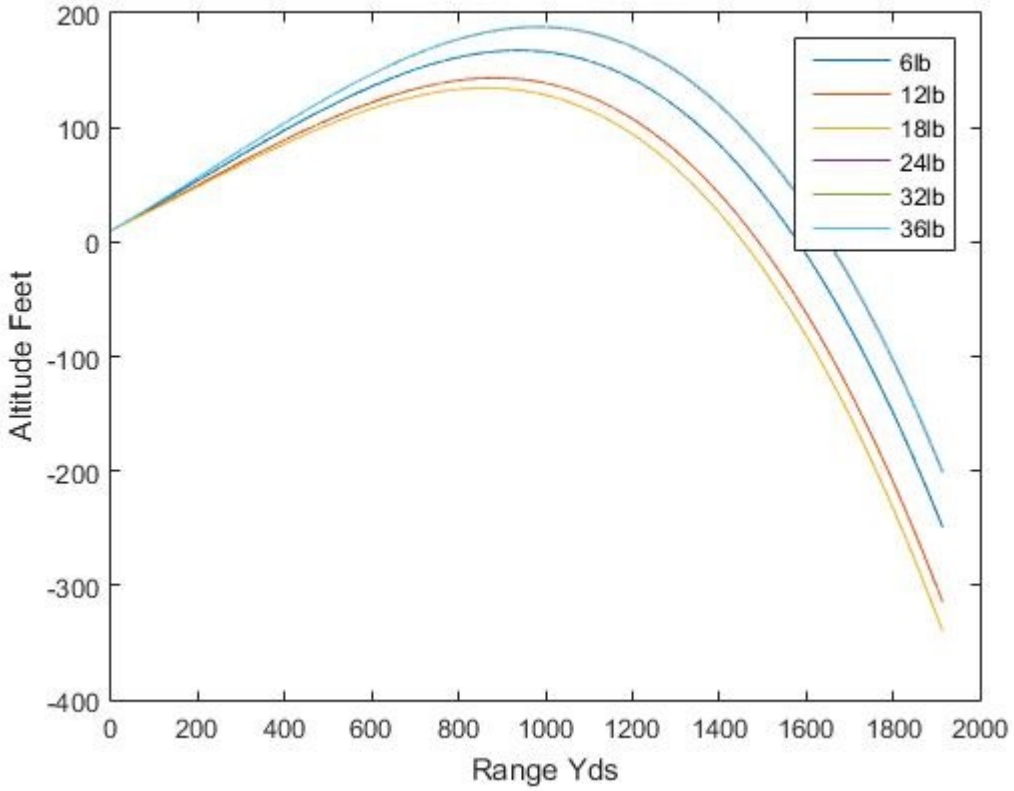

Figure 8: Altitude of the cannonball as a function of against the distance downfield

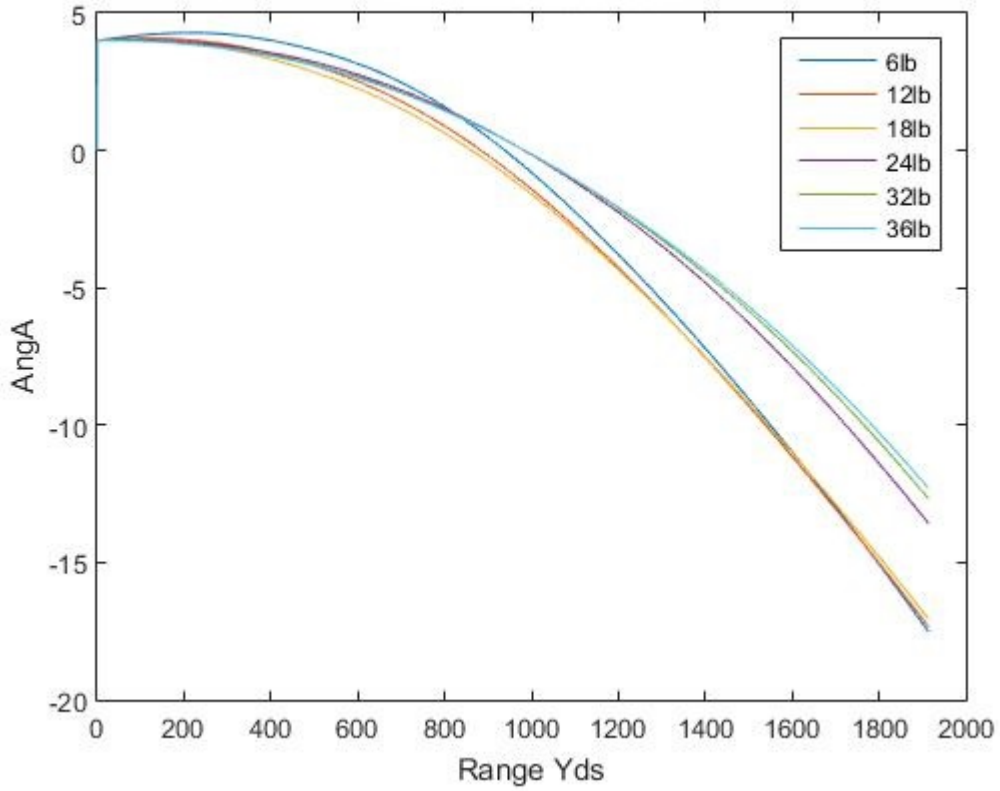

Figure 9: Angle of Attack (in degrees) of the cannonball as a function of against the distance downfield

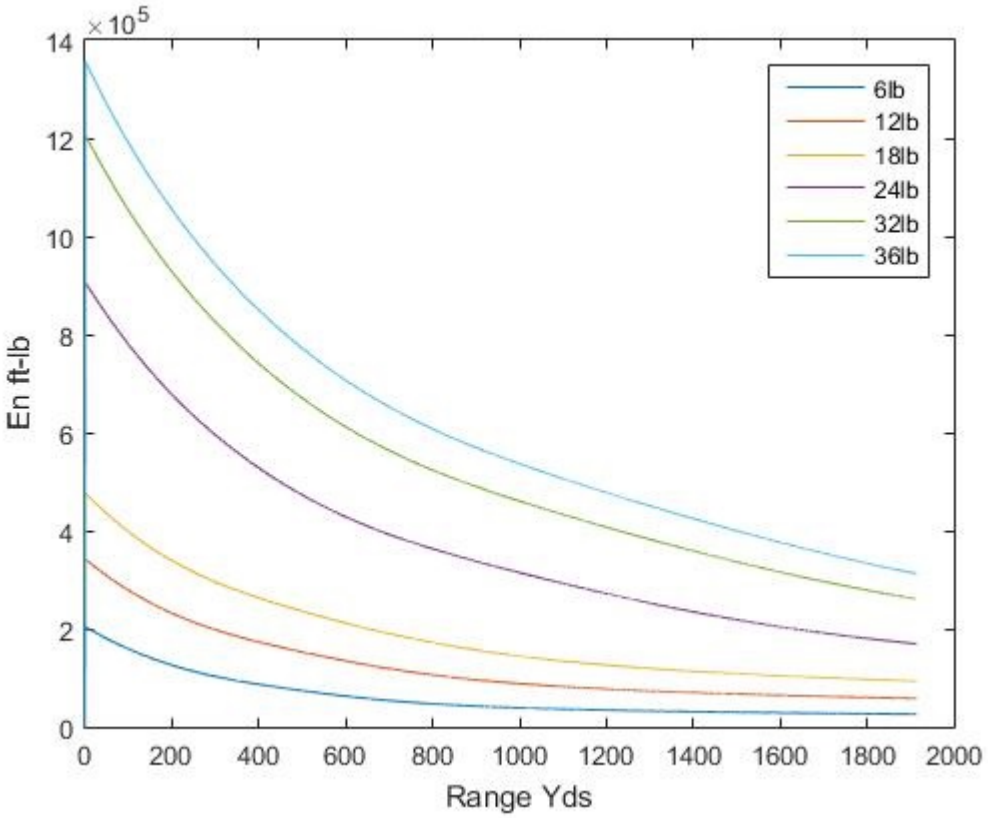

Figure 10: Kinetic Energy of the cannonball as a function of against the distance downfield

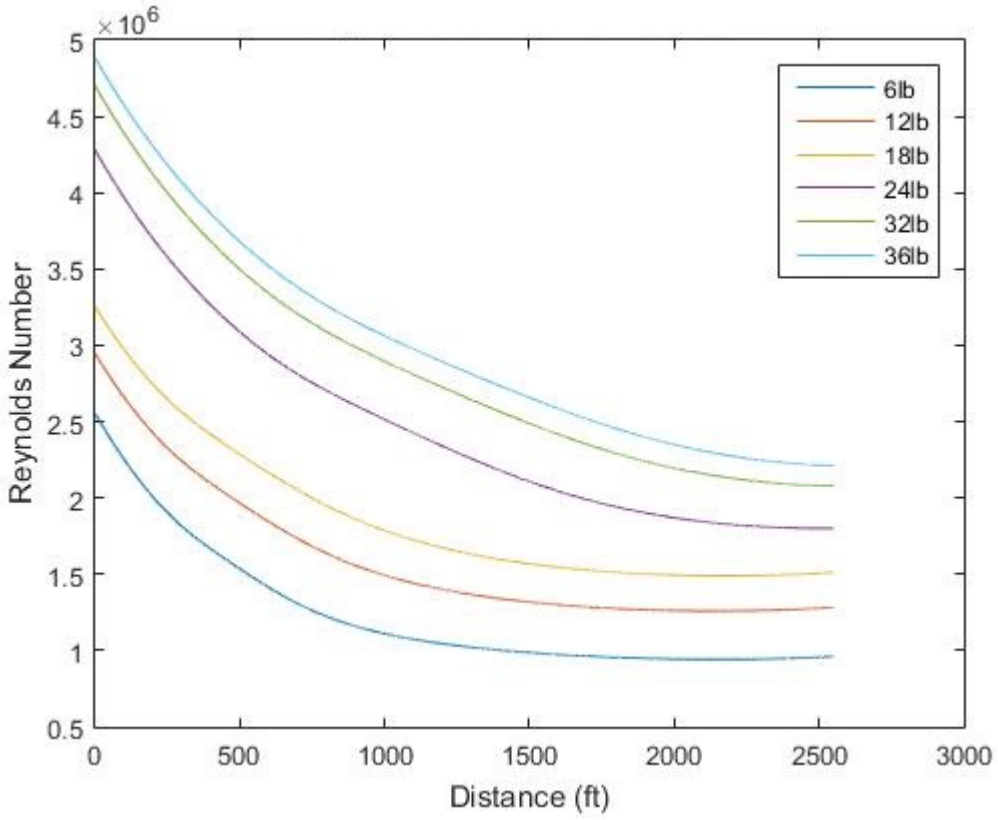

Figure 11: Reynolds number of the airflow around the cannonball as a function of against the distance downfield

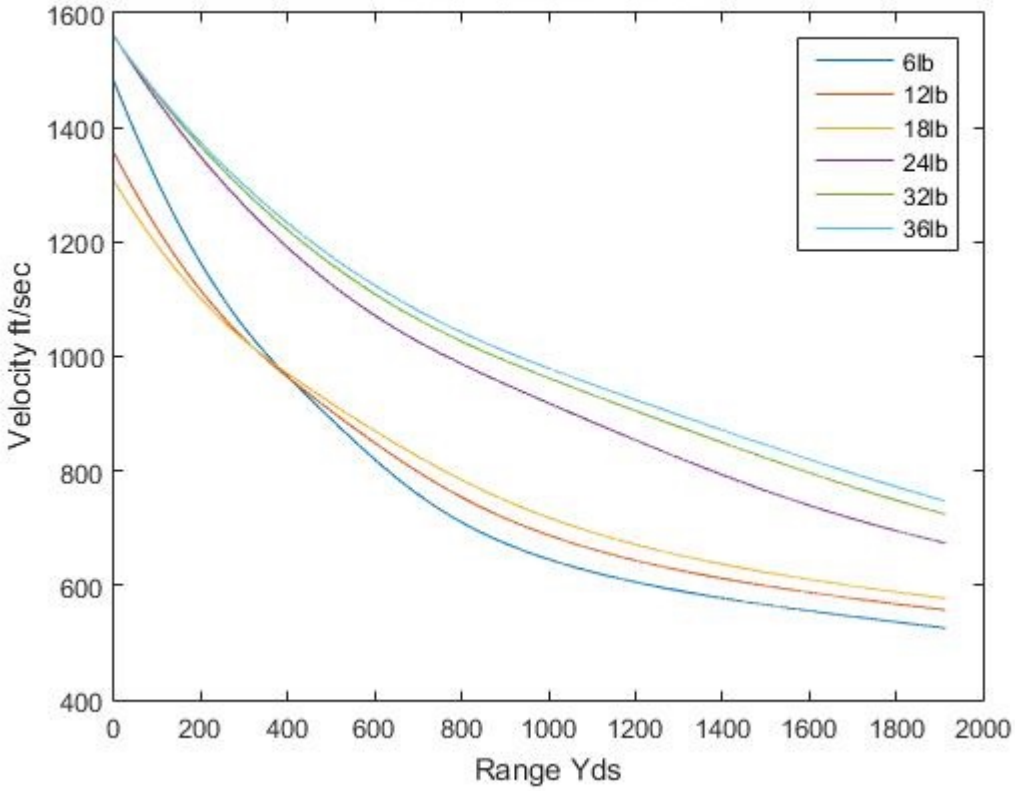

Figure 12: Total velocity of the cannonball as a function of against the distance downfield

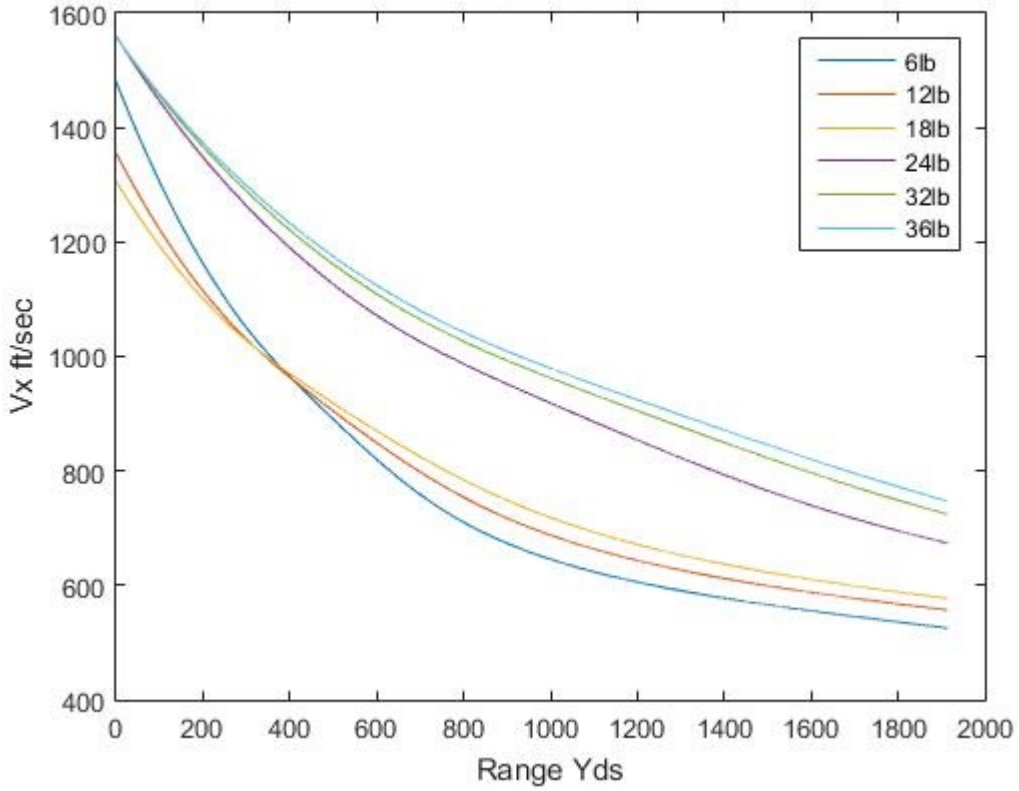

Figure 13: X-component velocity of the cannonball as a function of against the distance downfield

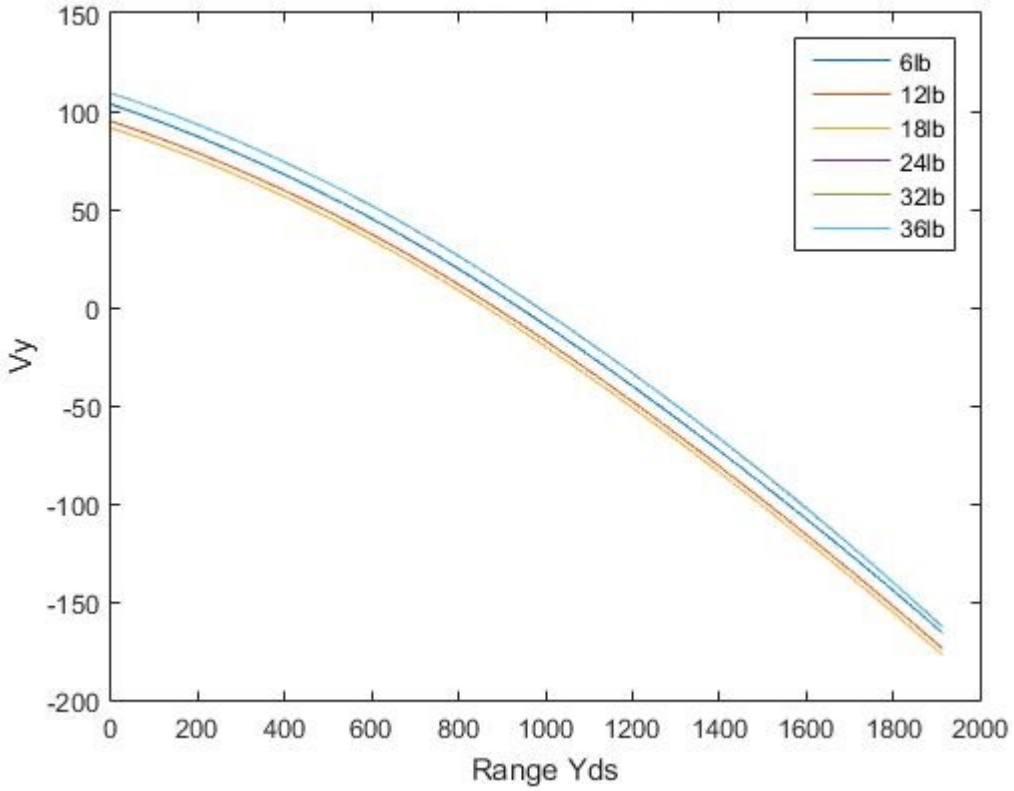

Figure 14: Y-component velocity of the cannonball as a function of against the distance downfield

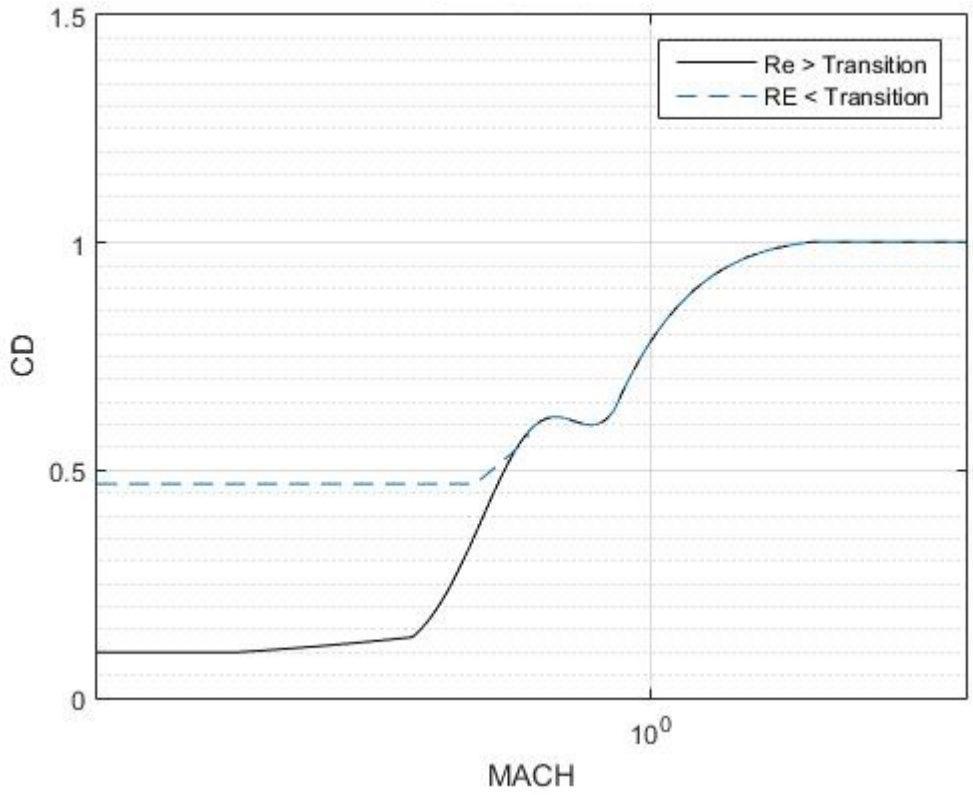

Figure 15: Coefficient of drag as a function of Mach number. The shown trend lines were used to approximate the drag for any given Mach number during flight. Modeled after the work done by Spearman and Braswell 1993.

Sensitivity Analysis for Cannonball Ballistics

Above results model the behavior of a cannonball in an idealized scenario: no wind, no rotation, no horizontal spread and a constant vertical angle. In order to answer the question "what lead to the inaccuracy of the cannon fire during the battle," scenarios need to be evaluated with less than ideal conditions.

Four scenarios were considered for assessment: the presence of a horizontal angle away from the target when firing, a non-preferred vertical angle when firing, variation in gunpowder quality, and a cross wind. An 18-pound cannonball with associated cannon size and gunpowder quantity was used for each study, and the changes in total velocity, x-component velocity, y-component velocity, kinetic energy, Reynolds number, landing position, altitude, angle of attack, and horizontal spread were used to analyze the impact of each scenario.

Horizontal Angle Modeling

The vertical angle used for firing was kept at 4 degrees, while the horizontal angle was varied from 0.1 to 2 degrees in increments of 0.1 degrees. A new z-component was integrated into the simulation, which alters how the total velocity and other velocity components are calculated. In 3D kinetics, the 3D vector must be projected onto a plane through which the desired component passes (Equation 17). For example, to calculate the x-component, the vector must be projected into either the x-y plane, or the x-z plane. The total velocity simply involves another square term (Equation 18).

$$V_z(0) = \cos(\alpha)\sin(\theta)\,V_{muzzle}$$

$$V_y(0) = \sin(\alpha)\cos(\theta)V_{muzzle}$$

$$V_x(0) = \cos(\alpha)\cos(\theta)V_{muzzle}$$

Equation 17: Vertical, downfield and horizontal components of the cannonball velocity at the first instant the cannonball leaves the muzzle

$$V_{total}(t_n) = \sqrt{v_z(t_n)^2 + v_y(t_n)^2 + v_x(t_n)^2}$$

Equation 18: Three-dimensional Total velocity of the cannonball at any point in time.

Horizontal angle errors can be generated either from operator error or improper support from the wooden platform below. The impulse generated from the cannon fire could wear the platform and cause the cannon to either sink into the damaged platform or ground, or change angle during fire.

Vertical Angle Modeling

The vertical angle at which the cannon was fired was varied from 3 to 5 degrees in 0.1 degree increments to see the variation in multiple parameters resulting from a 1-degree variation. All other parameters and equations were kept constant. The vertical angle could vary either due to improper setup by the operator or wear in the wooden platform causing the cannon to sink into either the ground or the wood, or tilt.

Gunpowder Quality Modeling

Gunpowder quality was varied from 1500 to 1600, known values for gunpowder quality in the 18th and 19th century as stated by Robins 1805, in increments of 100 to simulate either poor gunpowder packing in the muzzle or moisture. All other parameters and equations were kept constant.

Cross Wind Modeling

Addition of a cross wind incorporates another direction of drag as well as movement. The average maximum wind speed in August in Middletown, RI was found by NOAA to be 15 miles per hour, and drag coefficients for that speed were found using the same model implemented in the original simulation. The drag force acting in the z-direction was considered using the relative

velocity of the cannonball to the cross wind. The same total velocity equation seen in Equation 18 was used to approximate the total velocity of the cannonball.

Results from Each Scenario

The standard deviations of the key parameters identified in the introduction to the sensitivity analysis can be seen in Table 1. Standard deviations for velocity, energy, altitude and angle of attack are based on the maximum value found in each simulation.

	Standard Deviations							
Assessment	Total Velocity (ft/s)	Y-Velocity (ft/s)	X-Velocity (ft/s)	Kinetic Energy (ft-lb)	Reynolds Number	Landing Position (ft)	Altitude (ft)	Angle of Attack (degrees)
Horizontal Spread	0.001	0.018	0.254	185.586	518.119	0.988	0.048	0.000
Vertical Angle	0.000	13.488	0.957	698.457	13546.083	657.614	38.441	0.607
Gunpowder Quality	14.112	0.984	14.077	10344.912	6723.339	47.127	2.710	0.000

Table 1: Standard deviation of key parameters for the various assessment scenarios.

Table 2 below shows the maximum and minimum Reynolds numbers within the simulations, as well as the maximum change in landing position downfield.

Assessment	Max. Reynolds Number	Min. Reynolds Number	Max. Change in Landing Position (ft)
Horizontal Spread	3254892.615	1419526.945	0
Vertical Angle	3254892.615	1337555.231	1141.079
Gunpowder Quality	3330076.747	1357272.55	229.0123

Table 2: Values of Key Parameters for the various assessment scenarios

Additionally, firing the cannon at an angle causing horizontal spread lead to a maximum 500-foot difference a 0.1-degree angle to a 2 degree angle. Rather than only use the 18-pound cannonball for the cross wind, each cannon with their associated cannonball and gunpowder quantity was used in the simulation. For comparison, only the results from the 6-pound cannonball are listed in Table

3. Values shown in the table are the differences between the cross wind simulation and the original simulation rather than standard deviations, for the speed of the cross wind was kept constant at 15 miles per hour.

Parameter	Difference
Min. Reynolds Number	-169.984
Max. Reynolds. Nummber	0
Landing Position (ft)	6
Horizontal Spread (ft)	13.102
Altitude (ft)	0.14
Angle of Attack (degrees)	0.000786

Table 3: Values of the differences between the original cannon simulation for the 6-pound cannonball and the simulation including a cross wind.

Analysis and Conclusions

The minimum Reynolds number for all simulations ensures the validity of the underlying assumptions made in this report. The cannonball avoids the drag crisis during external ballistic performance, and the pressure drag is the dominant force acting on the cannonball. Additionally, the standard deviations of the total velocity are very small in comparison to the speed of sound. The assumption that the projectile is moving at supersonic speed and, thus, rotational forces can be neglected is also verified since the original simulation found this assumption valid.

As expected, changing the vertical angle at which the cannon is fired causes the largest changes in key parameters. Properly adjusting the angle at which the cannon is fired for the desired landing position downfield is crucial for hitting a target. Insufficiently-trained militia men may have encountered misses from improper angle selection due to inexperience. Additionally, as stated previously, damage to the wooden platform beneath the cannon could cause changes in vertical angle.

Variations in gunpowder quality also caused significant variations in landing position: a difference of about 230 feet. Quality can change depending on manufacturing, as well as storage. Improperly storing the gunpowder such that moisture contaminates the powder could change the performance of the cannon, as seen by the results. Middletown, Rhode Island air is higher in moisture content due to coastal environment; therefore, there is an increased chance for moisture to contaminate the gunpowder if not stored properly.

While horizontal angle did not cause a change in downfield landing position in the x-direction by more than about a foot, there was a large window of error for landing position in the z-direction (left and right when facing downfield), specifically 500 feet when fired at a four-

degree vertical angle. Changes in horizontal angle can occur from the same sources as the vertical angle: inexperience and platform damage.

The presence of a cross wind perpendicular to the desired trajectory of the cannonball does produce some undesired flight trajectory elements. The cannonball did land 6 feet short of the target, as well as about 13 feet to the right of the center of the target. It is worth noting, though, that the speed of the wind was based on the average maximum wind speed in August for Middletown, Rhode Island. The wind speed was not likely at this maximum while every cannonball was fired. Wind speed could have also been higher than average at that time. Regardless of the exact speed of the cross wind, the presence of a cross wind causes the smallest changes in performance but could be just enough to miss a target.

In conclusion, the vertical angle at which the cannon is fired and gunpowder quality cause the largest changes in ballistic performance when firing a cannon.

References

1. Bush, J. W. M. 2013 “The aerodynamics of the beautiful game” MIT, department of mathematics. Web. Accessed May 21, 2016. http://math.mit.edu/~bush/wordpress/wp-content/uploads/2013/11/Beautiful-Game-2013.pdf
2. Collins, A. R. n.d. “Smooth Bore Cannon Ballistics” Australian Research Council. Web. Accessed May 21, 2016. http://arc.id.au/CannonBallistics.html
3. Lumin. Z. 1992 “Research on the Assymetrical Aerodynamic Forces of Reentry Vehicles” Foreign Technology Division, Translation Division. China.

4. Porche, D., George, P. n.d. “Solid Shot Essentials: A Guide to the Authentic and Non-Authentic” Web. Accessed May 21, 2016. http://www.pochefamily.org/books/solidshotessentialsmod.html
5. Robins. B. 1805 “New Principles of Gunnery Ed 2” London.
6. Spearman, M. L., Braswell, D. O. 1993 “Aerodynamics of a sphere and an oblate spheroid for Mach numbers from 0.6 to 10.5 including some effects of test conditions” NASA Technical Memorandum 109016. Hampton, Virginia.

Trajectory of a Cannonball by Dr. Stephen A. Jordan

TRAJECTORY OF A CANNONBALL

By

Dr. Stephen A. Jordan
Jordan Engineering
Narragansett, RI 02882
www.idocfd.com

Summary: The present report is an engineering analysis of cannonballs (shots) launched from a cannon barrel typical of the revolutionary war. First attempts assumed ideal conditions meaning that the shot was smooth with no rotary motion at launch. During ideal flight, an opposing aerodynamic drag and a vertical gravitational acceleration were the prime input parameters to a 2^{nd}-order time-dependent numerical computation of the shot trajectory. The aerodynamic drag was calculated by a semi-empirical expression in terms of the instantaneous shot Mach and diameter-based Reynolds numbers. By adhering to the historical data, the ideal computations involved four combinations of a constant shot/charge weight ratio. Comparisons between the ideal trajectories and historical range data showed largest differences at the lowest launch angles (0° to 10°). But a consistent outcome revealed the surrounding flow as strictly supercritical (fully turbulent). Attempts to reduce the range-data disparity began with treating the shot's rough surface. Knowing that the cannonballs were formed inside a sand/clay/water mixture mold, the aerodynamic drag coefficient was modified accordingly which produced an overall higher resistive force during shot flight. The differences in the range data comparisons reduced substantially where the highest launch angle (10°) was under 4%. A second improvement in the trajectory simulation involved the shot's rotary motion. This added effect gave an initial angular velocity and acceleration at shot launch. Moreover, the computation extended to a three-dimensional spherical system to account for out-of-plane (2D) rotary motions. New comparisons between the numerical and historical range data revealed logical trends in the shot trajectory. The shot consistently missed the intended target with rise in launch angle until reaching a peak lateral distance (~ 50 yards) at 8°. Future efforts to improve predictions of the shot trajectory rest on the highly complex interaction between the shot's rotary motion and the oncoming freestream flow.

TRAJECTORY OF A CANNONBALL

The following white paper is a brief engineering study of a cannonball (called shot) fired from a cannon typical of the revolutionary war. Under ideal conditions, the shot trajectory would be two-dimensional (2D)- traveling horizontally and vertically giving an arc-type shape. Ideal conditions in this sense describe a perfectly-spherical shot launched through a frictionless cannon barrel of known length at a fixed angle relative to the horizontal axis (ground level). Frictionless implies a shot launched with no circumferential spin. The launch initiates from an impulsive force delivered by an instantaneous explosion (delta function) of compacted gun power behind the shot. As the shot traverses towards the intended target, its trajectory is affected only by a resistive

aerodynamic drag force and a vertical gravitational acceleration. We will begin this study assuming ideal conditions with comparisons to experimental data in terms of distance traveled by the shot under varying parameters of shot weight, gun power weight and launch angle. Units of each material property and launch parameter will adhere to the Imperial (or US customary) system (lb., ft. and sec).

The launch dynamics of the cannon shot begin with the impulsive force (F). The initial velocity of the shot at time t = 0 is $m_s v_o = \sum F_{0\text{-}1} = m_s v_1$ where m_s and v are the shot mass and shot velocity. Because the force is an impulse and the initial velocity v_o is zero, the launch velocity is simply $v_1 = F/m_s$. However, this ratio for estimating v_1 is not immediately useful because no experimental data exists for the impulsive force. Instead, an alternate expression was developed by Robins[1] involving the impulsive force distributed over the total barrel length (L). Accordingly, this approach required a kinetic energy balance of the form $m_s v_1^2 = 2\int_l^L F(s) + m_s v_0^2$ for determining the shot launch velocity with F(s) evaluated by the expression F(s) = RpAℓ/s where R, p, A, ℓ and s are the ratio of hot gas pressure to atmospheric pressure, atmospheric pressure, barrel area (or bore) and gun power length within the barrel length (s); $0 \leq s \leq L$. After substituting this force definition into the energy balance equation, integrating along s, then simplifying, the amplitude of the launch velocity becomes[2]

$$v_1^2 = \frac{2Rp}{m_s} l\pi r^2 \ln\left(\frac{L}{\ell}\right) \qquad \text{(Eq. 1)}$$

where r is the bore (or shot) radius. The length ℓ is given by $\ell = m_p/(\pi r^2 \rho_p)$ with m_p and ρ_p as the mass and density of the gun power. For the present calculations, p = (14.7)(144) lb/ft^2 and ρ_p = 55lb/ft^3. Robins[1] measurements provided R = 1000, but the later experiments by Hulton[1] suggested 1500 < R < 1600. In the present calculations, we will use the latter value (R = 1600). Lastly, we note that the position direction of the launch velocity (v_1) is coincident with the longitudinal axis of the cannon barrel.

Given the launch velocity, the next step demands obtaining a useful expression for the aerodynamic drag force (F_a) acting on the spherical shot during flight. The position vector of this drag force aligns with the shot's local trajectory, but opposes the corresponding direction of the flight velocity vector (v_s). According to our conventional definition, $F_a = 1/2 C_D \rho_a A v_s^2$ where C_D, ρ_a and A are the aerodynamic drag coefficient, air density and shot cross-sectional area. Herein, we emphasize that the drag coefficient C_D of a sphere is not a simple determination. This parameter is highly dependent on the trajectory Mach number (M_a) and the Reynolds number (Re_D) as illustrated in Fig. 1; $M_a = v_s/a$ and $Re_D = 2v_s r/\upsilon$ where a and υ are the speed of sound and the kinematic viscosity at local atmospheric conditions. Experimental measurements show that the effects of Re_D on C_D become negligible at high values of M_a and vice versa. Unfortunately, the trajectory of a cannon shot covers the full range of these coupled parameters. After many experimental and analytical studies,

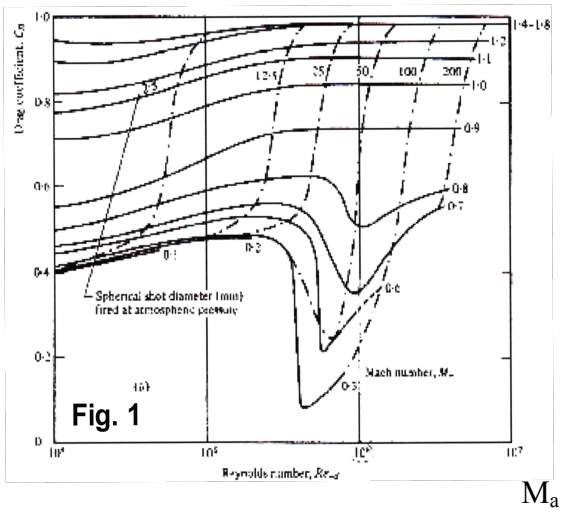

Fig. 1

resultant formulations and procedures for estimating the coupled effects of M_a and Re_D on the aerodynamic drag coefficient C_D have become reasonable reliable.

The procedure adopted herein for evaluating C_D adheres to the collected works of Miller and Bailey[2] and Morrison[3] as described by Collins[4]. According to Morrison[3], C_D for a smooth sphere can be estimated in terms of only Re_D at low-Ma ($M_a < 0.3 \rightarrow$ incompressible flow conditions) by the semi-empirical expression

$$C_{D'}(Re_D) = a/Re_D + b(Re_D/B)/[1.0+(Re_D/B)^{\alpha}] + c(Re_D/C)^{\beta}/[1.0+(Re_D/C)^{\lambda}] + Re_D^{\delta}/D \quad \text{(Eq. 2)}$$

where $a = 24$, $b = 2.6$, $B = 5.0$, $\alpha = 1.52$, $c = 0.411$, $C = 263{,}000$, $\beta = -7.94$, $\lambda = -8.0$, $\delta = 0.8$ and $D = 461{,}000$. This expression is graphically illustrated in Fig. 2 for $10^4 \leq Re_D \leq 10^7$ with the following limits;

$$Re_D \geq 2.0\text{x}10^6 \rightarrow C_{D'} = 0.15$$
$$1.20\text{x}10^6 \leq Re_D < 2.0\text{x}10^6 \rightarrow C_{D'} = 0.19 - 8\text{x}10^4/Re_D$$
$$4.77\text{x}10^6 \leq Re_D < 1.2\text{x}10^6 \rightarrow C_{D'} = -0.485 - 0.1\cdot\log(Re_D)$$

In view of Fig. 2, $Re_D < 3.5\text{x}10^5$ identifies a subcritical state (laminar flow surrounding the shot), $3.5\text{x}10^5 \leq Re_D \leq 4.2\text{x}10^5$ as critical (transitional flow) and $Re_D > 4.2\text{x}10^5$ as supercritical (turbulent flow).

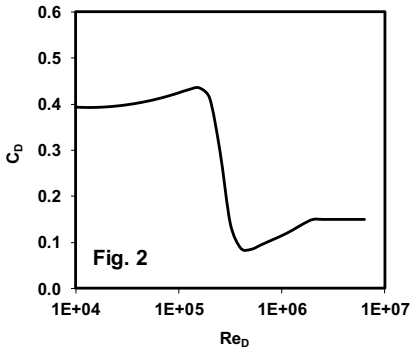

Fig. 2

The impact of M_a as well as the coupled effects of M_a and Re_D are modeled using cubic Benzier functions. These functions appear as

$$B_a(u) = a_1\cdot(1-u)^3 + 3a_2\cdot u\cdot(1-u)^2 + 3a_3\cdot u^2\cdot(1-u) + a_4\cdot u^3 \quad \text{(Eq. 3a)}$$

$$B_b(u) = b_1\cdot(1-u)^3 + 3b_2\cdot u\cdot(1-u)^2 + 3b_3\cdot u^2\cdot(1-u) + b_4\cdot u^3 \quad \text{(Eq. 3b)}$$

with the variable u ranging as $0 \leq u \leq 1$. The coefficients a_i are four points that target M_a whereas the coefficients b_i target C_D. An example at high M_a where the Re_D influence becomes negligible on C_D produces the coefficients $a_i = (0.1, 0.95, 0.55, 1.5)$ and $b_i = (0.0, 0.0, 0.95, 1.0)$. The last two coefficients denote $C_D = 1.0$ when $M_a = 1.5$ ($u = 1$). Thus, the limit $M_a = \min(1.5, Ma)$ is necessary to implement Eqs. 3. Likewise, the first two coefficients (0.1, 0.0) create the limit $M_a = \max(0.1, Ma)$ where M_a no longer influences C_D. For $M_a = B_a = 0.1 \rightarrow 1.5$, the variable u is determined iteratively under an error tolerance (~0.001) followed by $C_D = B_b$ given u. When $M_a < 1.5$, the impact of Re_D is introduced using the coefficients $g_i = (0.0, 0.85, 0.57, 1.0)$ and $h_i = (1.1, 1.1, 0.05, 0.0)$ for the Benzier functions $B_g(u)$ and $B_h(u)$. Again, u is iteratively evaluated for $B_g = M_a$ followed by B_h knowing the variable u. Combining these Benzier functions with Eq. 2 gives the relationship

$$C_D = B_b(u) + B_h(u)\cdot C_{D'}(Re_D) \quad \text{(Eq. 4)}$$

Beside raising the drag coefficient, $M_a > 0.1$ shifts the C_D curve in Fig. 2 to the right along the Re_D axis (see Fig. 1). This shift is handled by the approximation

$$S(M_a) = s_1 + s_2 \cdot \tan^{-1}[s_3 \cdot (M_a - s_4)] \quad \text{(Eq. 5)}$$

where $s_i = (0.78, 0.22, -12.0, 0.23)$. Thus, the final expression for estimating C_D is

$$C_D = B_b(u) + B_h(u) \cdot C_{D'}[S(M_a) \cdot Re_D] \quad \text{(Eq. 6)}$$

This relationship is graphically illustrated in Fig. 1 for $0.3 \leq M_a \leq 1.5$ and $10^4 \leq Re_D \leq 10^7$ (see Miller and Bailey[2] for additional details).

Knowing the aerodynamic drag force (F_a) and the initial velocity (v_1), we can formulate the trajectory path of the shot during flight. According to Newton's 2nd law $F_a = m_s a_s$ where a_s is the shot acceleration during flight. Using the variable $f_s = s_s$ where s_s is the shot arc distance, then $ds_s/dt = f_s' = v_s$ and $f_s'' = d^2s_s/dt^2 = [a_s - g \cdot \sin(\theta)]$ such that Newton's law becomes a 2nd-order ordinary differential equation (ODE) written as

$$f_s'' + \Lambda f_s'^2 = 0 \quad \text{(Eq. 7a)}$$

where $\Lambda = 1/2 C_D \rho_a A/m_s$, g is the vertical gravitational acceleration (32.2 ft/s^2) and θ is the local angle of the trajectory path referenced to the horizontal axis (ground level). Equation 7a can be readily advanced temporally using a 4th-order Runge-Kutta method from time t = 0. The horizontal (x) and vertical (y) components of Eq. 7a are

$$f_x'' + \Lambda f_s' f_x' = 0 \quad \text{(Eq. 7b)}$$

$$f_y'' + \Lambda f_s' f_y' = 0 \quad \text{(Eq. 7c)}$$

with $f_s' = (f_x'^2 + f_y'^2)^{1/2}$, $\theta = \tan^{-1}(f_y'/f_x')$ and $f_y'' = a_y - g$. The solution sequence for calculating the shot trajectory proceeds as Eq. 1 [$f_s'(t=0) = v_1$], Eqs. 3, 5 and 6 [$C_D(t)$] and Eqs. 7 [$s_s(t)$, $x_s(t)$, $y_s(t)$, $v_s(t)$, $v_x(t)$ and $v_y(t)$] with fixed time step dt = 0.01. The computation terminates when $y_s \leq 0$. The air density was $\rho_s = 0.0023$slugs/ft^3 which was modified by the shot altitude according to $H(y_s) = e^{-\kappa y_s}$ with $\kappa = 3.158 \times 10^{-5}$.

Table 1 Historical Range Measurements Listed by Collins[4]

Measured Range (yds)											
Shot Weight (lbs)-	Launch Angle (θ_1°)										
Charge Weight (lbs)	0	1	2	3	4	5	6	7	8	9	10
12-4	300	700	913	1189	1400	1580	1800				2330
12-4			1000			1520					
24-8	297	720	1000	1240	1538	1807	2023	2100	2498	2638	2870
24-8			1100			1854					2600
32-10	350	750	1050	1320	1600	2085	2100	2200	2460	2600	2900
32-10			1130			1964					2682
42-14	400	1045	1263	1622	1770	1938	2100	2300	2580	2650	2900

Collins[4] extracted forty-nine trajectory measurements (see Table 1) from two 19th-century British experimental studies on the shot trajectory at four sets of shot (W_s) and charge (W_c) weights that were launched at eleven angles ($0° \leq \theta_1 \leq 10°$). The ratio $S_c = W_s/W_c \sim 3$ was the standard service charge ratio which produced a consistent launch velocity ($v_1 \sim 1685$ft/s). Figure 3 shows four shot paths for the same launch angle $\theta_1 = 6°$. In that figure, the notations signify the shot and charge weights as W_s-W_c. Notice that the higher shot and charge weights generate longer trajectory ranges. Apparently, the elevated drag force due to the increased diameter of the larger shot is offset by the shot mass; that is $\Lambda = F_a/m_s$ decreased with consistent S_c and v_1.

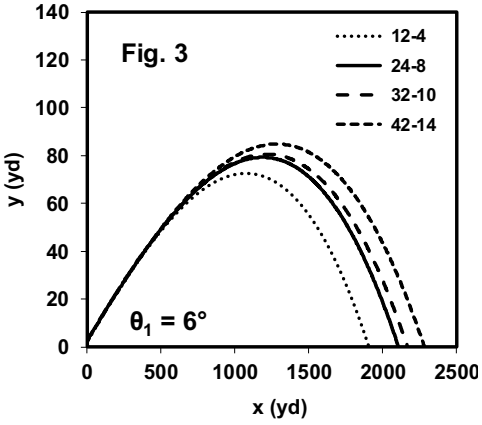

Listing comparisons between the historical experimental measurements and the present numerical predictions of the shot ranges under assumed ideal conditions is futile at this point. Instead, plotting their percent differences in terms of the required F_a to reach agreement is more appropriate to better understand the contributing factors leading to realistic conditions. Inasmuch as C_D is the only adjustable quantity, we will focus on that applied force parameter. Figure 4 shows a C_D factor (in percent) against the shot launch angle (θ_1) for the four sets of shots and charges. To be perfectly clear, the C_D factor (C_{DF}) in the figure is the additional drag force coefficient (or percent drag D_s) that is necessary to reach agreement between the experimental range measurements and the present numerical predictions; $\Lambda(C_D) = \Lambda[C_D \text{ (Eq. 6)}] + \Lambda(C_{DF})$. Looking at Fig. 4, the only immediate observation is the reduction of C_{DF} with higher θ_1.

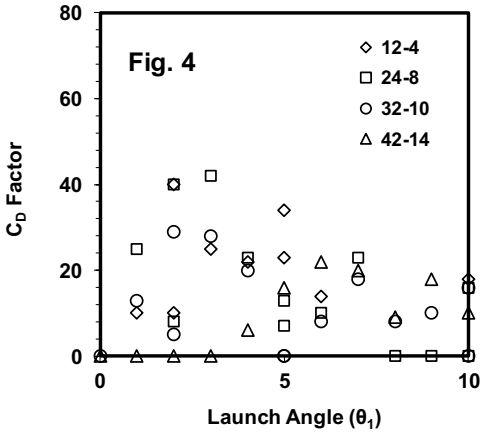

The first deviation from ideal conditions that is worth investigating is the shot's assumed smooth surface. Reports[5] of cannon balls recovered without several centuries of environmental degradation indicate a sand surface roughness. This discovery is certainly acceptable because the cannon ball molds were constructed of a coarse sand mixed with clay and water. Sand surface

roughness is sized ε ~ 1mm. Scaling this value by the various cannon ball diameters (3in < D < 7in) gives $5.0x10^{-3} < \varepsilon/D < 1.3x10^{-2}$. Figure 5 shows the resultant shift in the drag coefficient curve (Fig. 2) in the form of increasing ε/D versus Re_D. According to the computations of the four sets of shot-charge weights and eleven launch angles under ideal conditions, minimum Reynolds numbers (at the target point $y_s = 0$) varied $1.5x10^6 < Re_D \leq 5x10^6$. Knowing that $Re_D > 10^6$, the shot flight is always in a supercritical state meaning that the surrounding flow condition is fully turbulent with a non-shedding vortical wake. Small surface imperfections such as the mold seam, filler hole sprue and mold vent sprue would most likely have little impact on the flight flow parameters. Moreover, $\varepsilon/D > 5x10^{-3}$ suggests that $C_{D'} \geq 0.4$ regardless of the coupled conditions of M_a and Re_D during flight (see Fig. 5).

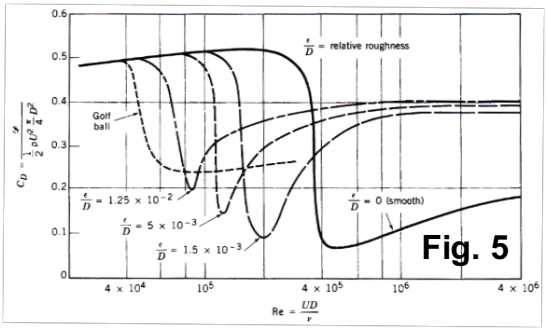

Fig. 5

Upon applying the restriction $C_{D'} \geq 0.4$ in Eq. 6, Fig. 6 shows the modified C_D factors for the shot-charge weights and launch angles in Table 1. The trend of a decreasing C_D factor with increasing launch angle (θ_1) that was previously observed in Fig. 4 is much more pronounced in this figure. At a launch angle $\theta_1 = 10°$, direct comparisons between the field range measurements and numerical predictions are within 5%. Although one should expect cannon preparation subtleties that would affect the shot launch and resultant trajectories, their disparities would not discount the recognizable trend between the C_D factor and the launch angle.

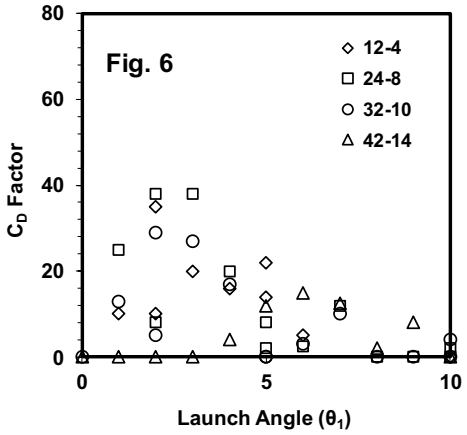

A second deviation from ideal conditions is circumferential spin of the spherical shot at launch. Circumferential spin would in fact be faster with lower launch angle under equivalent shot and charge weights due to the increased effect of wall friction while the shot transverses the cannon barrel. Unlike the longitudinal motion, the shot would experience both an angular velocity (ω_s) and acceleration (α_s) at launch. Assuming that the spherical shot is rolling and sliding while traversing the cannon barrel, we can readily approximate ω_s and α_s in the following manner. Looking at Fig. 7, the frictional force (F_θ) is $F_\theta = \mu_k \cdot N = \mu_k \cdot W \cdot \cos(\theta)$ with μ_k as the kinetic (sliding) friction coefficient. By applying Newton's 2nd law at the sphere center, the shot acceleration becomes $F_\theta \cdot r = I \cdot \alpha$ where I is the sphere's moment of inertia. Given that $I_{sphere} = 2/5 m_s \cdot r^2$ and $W_s = m_s \cdot g$, the shot's angular acceleration (α_1) at launch is

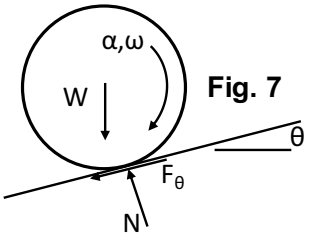

Fig. 7

$$\alpha_1 = 5\mu_k \cdot g \cdot \cos(\theta_1)/2r \qquad \text{(Eq. 8)}$$

with the angular velocity $\omega_1 = \alpha_1 \cdot t_1$. The variable t_1 is the time the shot traverses the cannon barrel. Again, by assuming an impulsive force at time $t_0 = 0$ and initial distance $s_0 = 0$ we can easily formulate t_1 as $s_1 = s_0 + v_1 t_1 + \frac{1}{2} a_1 t_1^2$. The acceleration a_1 at launch is $F_\theta = m_s \cdot a_1$ (Newton's 2nd law) or $a_1 = \mu_k \cdot g \cdot \cos(\theta_1)$. Knowing the launch velocity from Eq. 1, the time t_1 is calculated using

$$t_1 = -v_1/a_1 + [(v_1/a_1)^2 + 2s_1/a_1]^{1/2} \quad \text{(Eq. 9)}$$

Engineering tables list $\mu_k \sim 0.2$ for dry sliding contact between two cast-iron surfaces. This parameter ranges between 0.48 and 0.55 for dry sandblasted surfaces. For the present calculations of the spherical shot traversing the cannon barrel, the sliding friction coefficient was set to 0.5.

An example calculation of $v_1 \sim 1683$ft/s and $\theta_1 = 6°$ for a 12-lb shot and 18-caliber cannon shows $t_1 = 0.0041$sec with $\alpha_1 = 211\text{sec}^{-2}$ and $\omega_1 = 0.86\text{sec}^{-1}$. Thus, the rotation of a shot exiting the cannon barrel would be observable by the field team. This argument is supported by several historical reports on Naval gunnery where a particular report[6] notes that the shot experiences a 'peculiar rotary motion through the air'. One should expect that any surface discontinuities on the shot surface (such as the mold seam, filler hole sprue and mold vent sprue) would enhance the rotary motion while traversing the cannon barrel (material contact) as well as during flight (aerodynamic contact).

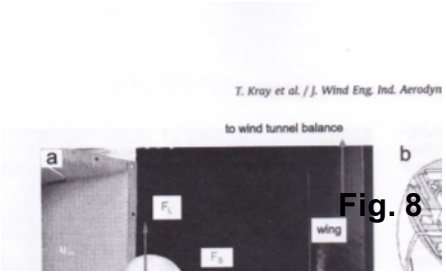

Fig. 8

A rotating sphere with an oncoming freestream will experience a lift force called the Magnus effect. Although Heinrich Magnus[7] reported this lift force in 1853, Walker (1671) noted much early the effect on a tennis ball as well as Robins (1742)[1] as a British artillery scientist. The Magnus force (F_M) is perpendicular to the drag force (F_D) as illustrated in Fig. 8 for an oncoming freestream from the left and a counter-rotating sphere[8]. Due to the resultant interaction between the oncoming freestream flow and sphere rotation, a positive Magnus force is a negative lift force (negative y-direction) as shown in Fig. 8. In the case of the cannon shot where the freestream is oncoming from the right with a clockwise rotation at an angle θ_1 from the ground level (x-axis), the positive Magnus force vector is directed -90° from the aerodynamic force vector (counter-clockwise is positive) or θ_1 - 90° from the x-axis. Notably, the combined effects of the flow state and rotational speed will lead to either a positive or negative Magnus force. According a report by Muto et al.[9], both the subcritical and supercritical states generate a positive Magnus force with minor dependence on the rotation rate. Conversely, the Magnus force becomes negative in the critical flow state with strong influence by the rotation rate. Knowing that the flow state of cannon shot is always supercritical, we can exploit the experimental measurements of Kray[8] and the computational results of Muto et al.[9] to access the Magnus effect on the shot trajectory.

According to Muto et al.[9] the Magnus force is positive and monotonically proportional to the spin rate (SP) when the sphere flow state is supercritical. This variable is defined $SP = \omega r/v_s$ which is easily evaluated at shot launch. After launch, dynamic interaction between the rotating sphere and oncoming freestream is incredibly complex and exceedingly difficult to reliably quantify in terms of a time-varying Magnus force during shot flight. To date, both the experimental measurements and numerical computations have reported the Magnus effect for constant spin rates and freestreams. Even under those constant conditions, very little data is available for the supercritical state. One option for assessing the Magnus effect on the present cannonball study is to assume an average force (or coefficient, C_{Mavg}) during flight. This average Magnus force can be readily quantified by iterative adjustments to the Λ variable in Eqs. 7 until close agreement is reached between $x_s(t)$ and the historical ranges listed in Table 1.

The Magnus force coefficient (C_M) holds a similar definition as the drag coefficient; $C_M = 2F_M/(\rho_a A v_s^2)$. Thus, the force variable becomes $\Lambda(C_{D,M}) = \Lambda[C_D \text{ (Eq. 6)}] + \Lambda(C_{Mavg})$ where (as before) $C_{D'} \geq 0.4$. Kray et al.[10] measured a near-linear relationship between C_M and SP with SP ≤ 0.3 for a soccer ball spinning in the supercritical regime. For our initial exercise, we will assume $C_{Mavg} = SP_{avg}$ with the sphere rotation being strictly 2D (along the x-y plane). Figure 9 plots the average spin rates necessary to reach agreement with the historical range measurements. The distribution of SP_{avg} data points indicate minimums when approaching the lowest and highest launch angles ($\theta_1 \rightarrow 0°$ and $\theta_1 \rightarrow 10°$). These results are quite reasonable because the smaller launch angles reach the target sooner (highest v_s, lowest F_M) whereas the larger angles launch the shot at the lowest spin rates (again lowest F_M). Negative average spin rates were found for about 15% of the test cases listed in Table 1. These opposite results are very reasonable when considering variabilities such as the shot surface roughness, cannon-shot-charge preparation, measurement error, etc.

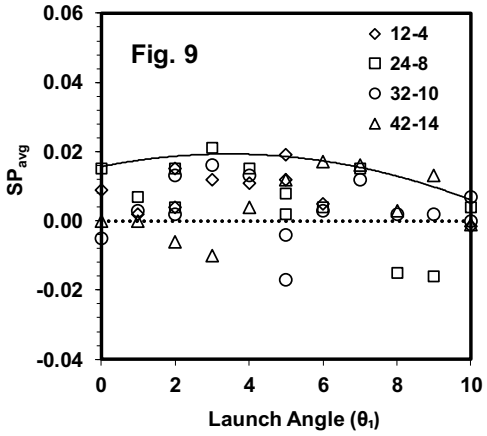

To continue our analysis of the Magnus effect, we will consider only the positive spin rates. Assuming that the rotation vector coincides with the x-y plane is obviously not realistic, but certainly not improbable. If we assume that these maximum positive SP_{avg} values represent x-y rotations, then they also define the spin rate envelope associated with 2D → 3D rotations. This envelope is illustrated in Fig. 9 as a 2nd –order polynomial (solid line); $SP_{avg} = d_1\theta_1^2 + d_2\theta_1 + d_3$ with $d_1 = -3.086\text{x}10^{-4}$, $d_2 = 2.128\text{x}10^{-3}$ and $d_3 = 1.556\text{x}10^{-2}$. Positive spin rates within the envelope represent a rotation vector in 3D spherical space. In spherical space, a second angle (φ_1) is required to position the rotation vector from the x-y plane. Again using the historical range data, we can approximate φ_1 from the four sets of shot-charge weights listed in Table 1. Evaluating φ_1 completes the present investigation for understanding the potential major factors contributing to cannon shots missing their intended targets.

The solution sequence in Eqs. 7 require additions and adjustments to treat a spherical trajectory path. A new lateral (z) coordinate is introduced of the form

$$f_z'' + \Omega f_s' f_z' = 0 \qquad \text{(Eq. 10)}$$

with the trajectory velocity (f_s') and new angle (φ_1) evaluated as $f_s' = (f_x'^2 + f_y'^2 + f_z'^2)^{1/2}$ and $\varphi_1 = \sin^{-1}(f_z'/f_s')$, respectively. In Eq. 10, $f_z = z_s(t)$ and $f_z' = v_z(t)$ which are the lateral distance and velocity of the shot trajectory path. The lateral acceleration component is f_z''. The new forcing function (Ω) is defined as $\Omega = 1/2 C_M \sin(\varphi_1)\rho_a A/m_s$ which becomes negligible ($\Omega = 0$) for a shot rotation vector coincident with the x-y plane. As before, we will assume $C_M = SP_{avg}$ with SP_{avg} defined by the 2nd-order polynomial. In Eqs. 7, the forcing function (Λ) for the x-y components of the trajectory path requires an adjustment as $\Lambda = 1/2 C_D \cos(\varphi_1)\rho_a A/m_s$ which reduces to a 2D solution of the trajectory path when $\varphi_1 = 0$. Although the variability of φ_1 during shot flight is most likely a non-linear function, no trajectory data exists to support a representative expression.

Thus, the present assessment of φ_1 assumes that this angle is constant (or average angle) during shot flight.

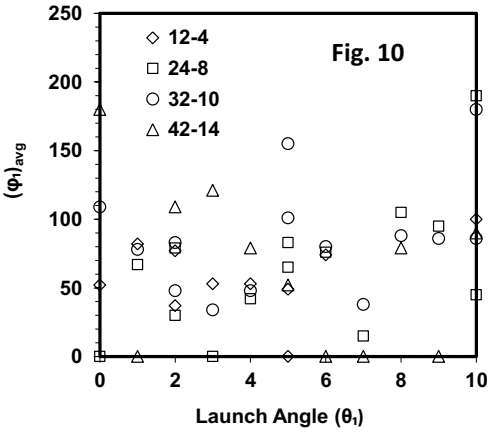

The estimated angles $[(\varphi_1)_{avg}]$ to account for the out-of-plane Magnus force vector are plotted in Fig. 10 versus launch angle (θ_1) Again, these angles arose from agreement between the trajectory predictions and historical range data listed in Table 1 that lie inside the Magnus force envelope. The condition $C_{D'} \geq 0.4$ was maintained throughout these determinations. The angles above 90° denote a negative Magnus force ($SP_{avg} < 0$ in Fig. 9) which may be possible when considering the complex interaction between the oncoming freestream and shot rotation. At first glance, the φ_1 angles generally increase with launch angle (θ_1) for each shot-charge combination. This result should be expected because the gravitational vector would induce the friction vector (F_θ) that represents contact between the shot and inside barrel to cause a more x-y planar rotation for the lowest launch angles. Notably, the φ_1 angles in Fig. 10 reveal a very large scatter for each launch angle. In many cases, the rotation vector varies between the x-y ($\varphi_1 = 0°$) and x-z planes ($\varphi_1 = 90°$). This particular result may reflect the non-uniformity of the shot surface. Inasmuch as the cannon bore was not much larger than the shot itself (windage $\leq$ 0.25 inches), surface imperfections such as the mold seam, filler hole sprue, mold vent sprue, rust and rough casting would play a contributing role in the initial direction of the shot's rotation vector. Seemingly, the large variability in the historical range data (even at equivalent launch angles) is probably attributed to the orientation of the Magnus force during shot flight.

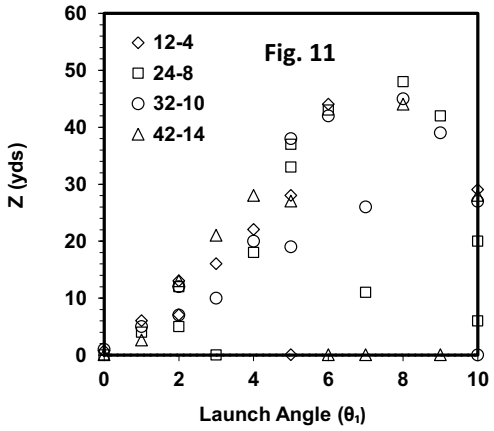

The lateral distances (z) from the x-y trajectory path that correspond to the φ_1 angles in Fig. 10 are plotted in Fig. 11. Of the forty-nine shots listed in Table 1, only nine shots (18%) show close proximity to the presumed targets in Table 1 (z < 1yd) even under the present analysis. A higher variability in the shot surface would reduce this accuracy percentage even further. The clear trend towards missing the intended targets is illustrated in Fig. 11 for the higher launch angles where 8° appears as the worst case. In the present analysis, a higher launch angle ($\theta_1 > 8°$) reduces the lateral variability due simply to the lower impact of the gravitational force on the angular velocity (ω).

Further improvements in the present prediction of the shot trajectory center on the complex interaction between the rotary motion and the high-speed freestream flow during flight to obtain a better quantitative understanding of resultant Magnus force. The available data used herein represents experimental measurements and numerical computations of the Magnus force at constant conditions of rotation rate and freestream velocity. But the Magnus force, rotation rate and oncoming freestream are all highly interactive and time-dependent. Fortunately, numerical strategies presently exist to quantify this time-dependent behavior. Building such a numerical strategy with an appropriate trajectory simulation matrix would require a couple of years to

finalize. But the final product would be ubiquitous meaning that one could accurately predict and clearly understand the shot's trajectory behavior which responds to the applied forcing during aerodynamic flight.

References

1. Robins, B., 1805, New Principles of Gunnery, 2nd Ed., London.
2. Miller, D.G. and Bailey, A.B., 1979, 'Sphere Drag at Mach Numbers from 0.3 to 2.0 at Reynolds Numbers Approaching 10^7,' *J. Fluid Mech.*, 93(3), 449.
3. Morrison, F.A., 2013, An Introduction to Fluid Mechanics, Cambridge University Press, New York.
4. Collins, A.R., 2012, Miscellaneous Technical Articles, Website www.arc.id.au.
5. Cvikel, D., Mentovich, E.D., Ashkenazi, D. and Kahanov, Y., 2013, 'Casting Techniques of Cannonballs from the AKKO 1 Shipwreck: Archaeometallurgical Investigation,' *J. Min. Metall. Sect. B-Metall.*, 49(1), 107.
6. Simpson, E., 1862, 'Treatise on Ordinance & Naval Gunnery', NY.
7. Magnus, H.G., 1853, 'On the Deviation of Projectiles: and on a Remarkable Phenomenon of Rotating Bodies', *Taylor's Foreign Scientific Memoirs*, Berlin.
8. Kray, T., Franke, J. and Frank, W., 2012, 'Magnus Effect on a Rotating Sphere at High Reynolds Numbers,' *J. Wind Engr. Ind. Aero*, 110, 1-9.
9. Muto M., Watanabe, H., Tsubokura, M., and Oshima, N., 2011, 'Negative Magnus Effect on a Rotating Sphere at around the Critical Reynolds Number', 13th European Turbulence Conference, *Journal of Physics: Conference Series*, 318, 032021.
10. Kray, T., Franke, J. and Frank, W., 2014, 'Magnus Effect on a Rotating Soccer Ball at High Reynolds Numbers,' *J. Wind Engr. Ind. Aero*, 124, 45-53.